A LETTERS JOURNAL EXPLORING THE FRONTIERS OF PHYSICS

Società Italiana di Fisica

edp sciences IOP Institute of Physics

LETTER

Multithermally invisible cloaks and sensors with complex shapes

To cite this article: C. Q. Wang *et al* 2021 *EPL* **133** 20009

A Letters Journal Exploring the Frontiers of Physics

January 2021

EPL, **133** (2021) 20009
doi: 10.1209/0295-5075/133/20009

www.epljournal.org

Multithermally invisible cloaks and sensors with complex shapes

C. Q. Wang[1], L. J. Xu[1(a)], T. Jiang[2], L. Zhang[3] and J. P. Huang[1(b)]

[1] *Department of Physics, State Key Laboratory of Surface Physics, and Key Laboratory of Micro and Nano Photonic Structures (MOE), Fudan University - Shanghai 200438, China*
[2] *Department of Radiology, Changhai Hospital, Naval Medical University - Shanghai 200433, China*
[3] *Key Laboratory of Materials for High-Power Laser, Shanghai Institute of Optics and Fine Mechanics, Chinese Academy of Sciences - Shanghai 201800, China*

received 1 November 2020; accepted in final form 22 December 2020
published online 22 March 2021

PACS 05.70.-a – Thermodynamics
PACS 81.05.Zx – New materials: theory, design, and fabrication

Abstract – Multithermal metamaterials are more practical to control thermal energy because there are three basic modes of thermal transport in nature. However, existing theories for multithermotics, such as the transformation theory and effective medium theory, are limited to complicated parameters or regular shapes. To solve the problem, we apply the thermal uniqueness theorem together with the heat flux conservation to design multithermal metamaterials including invisible cloaks and sensors. Multithermotics refers to the combination of conduction and radiation, which are described by the Fourier law and the Rosseland diffusion approximation, respectively. The present scheme can simplify parameters despite complex shapes, which only requires simple layered structures. We further perform finite-element simulations with different shapes to confirm the desired effects. These results provide guidance for multithermal management such as considering the combination of other basic modes of thermal transport.

Introduction. – Thermal transport has three basic modes including conduction, radiation, and convection. Since the proposal of transformation thermotics [1,2], conduction has been widely explored and well manipulated [3]. To make the transformation theory more realistic, radiation and convection have recently been considered, yielding multithermal (or omnithermal) metamaterials [4–10]. Multithermal (or omnithermal) refers to the combination of two (or three) basic modes of thermal transport. In addition to the transformation theory [4–10], the effective medium theory was also broadly explored [11–16]. Numerous novel phenomena based on several basic modes of thermal transport have been revealed such as anti-parity-time symmetry [17–19], thermal waves [20–22], and directional heat transfer [23].

However, existing methods also have some restrictions. We take thermal cloaking as an example. When the transformation theory is applied [4–10], the parameters are highly complicated with anisotropy, inhomogeneity, and even singularity. When the effective medium theory is used [11–16], the shapes are restricted to only ellipses or ellipsoids. These limitations may hinder engineering applications. To solve the problem, the uniqueness theorem [24] was developed to actively [25–29] or passively [30] control boundary conditions, but the scheme can only handle one basic mode of thermal transport (*i.e.*, conduction) so far. Therefore, it is of practical significance to establish the related method to design multithermal metamaterials without anisotropic, inhomogeneous, and singular parameters, and with complex shapes beyond the existing ellipses and ellipsoids.

For this purpose, we propose a mechanism based on the thermal uniqueness theorem and the heat flux conservation to design multithermally invisible cloaks and sensors. We consider the combination of conduction and radiation, which are described by the Fourier law and the Rosseland diffusion approximation [31], respectively. Invisible cloaks [32–35] can protect objects from infrared detection. However, the cloaked region has no feeling of external temperatures. Therefore, we further design invisible sensors [35–40], which can accurately detect local temperatures without distortions of background temperatures. Compared with existing methods

(a) E-mail: 13307110076@fudan.edu.cn
(b) E-mail: jphuang@fudan.edu.cn

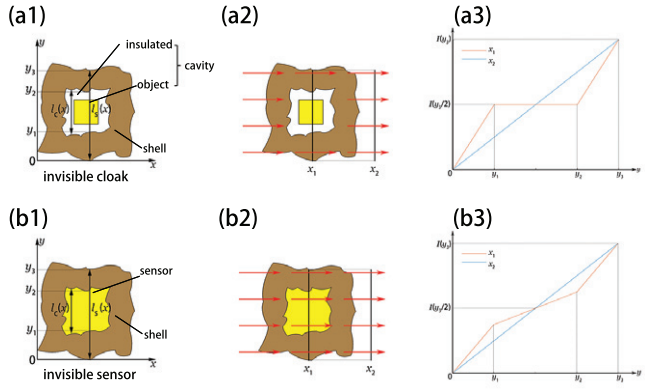

Fig. 1: Schematic diagrams of (a1)–(a3) invisible cloak and (b1)–(b3) invisible sensor with complex shapes. (a1) and (b1): structure and size. (a2) and (b2): heat flux distribution (denoted by red arrows). (a3) and (b3): line integration of the heat flux I as a function of position y on the black lines in (a2) and (b2).

[32–40], the present one only requires simple parameters and structures. Meanwhile, it has superior performance: for invisible cloaks (see fig. 1(a1)), all regions except the cloaked one are invisible; for invisible sensors (see fig. 1(b1)), all regions are invisible. This feature goes beyond existing methods [32–40] which cannot make the designed shells thermally invisible. In what follows, let us start from the theory.

Theory. – We consider conduction and radiation simultaneously, and the total heat flux $\boldsymbol{J}_{\rm total}$ includes the conductive flux $\boldsymbol{J}_{\rm con}$ and the radiative flux $\boldsymbol{J}_{\rm rad}$,

$$\boldsymbol{J}_{\rm total} = \boldsymbol{J}_{\rm con} + \boldsymbol{J}_{\rm rad}. \tag{1}$$

The conductive flux is given by the Fourier law,

$$\boldsymbol{J}_{\rm con} = -\kappa \nabla T, \tag{2}$$

where κ is thermal conductivity. The radiative flux is described by the Rosseland diffusion approximation,

$$\boldsymbol{J}_{\rm rad} = -\gamma T^3 \nabla T, \tag{3}$$

where $\gamma = 16/3n^2\sigma\beta^{-1}$ is the radiative coefficient, β is the Rosseland mean extinction coefficient, n is the relative refractive index, and σ is the Stefan-Boltzmann constant ($=5.67\times10^{-8}\,\mathrm{W\,m^{-2}\,K^{-4}}$). Equation (3) is on the assumption that the mean free path of photons is far smaller than the system size, so photons are featured by diffusion. This process also occurs in many practical materials like aerogels [41,42].

We then substitute eqs. (2) and (3) into eq. (1),

$$\boldsymbol{J}_{\rm total} = -\kappa\nabla T - \gamma T^3 \nabla T = -(\kappa + \gamma T^3)\nabla T. \tag{4}$$

We then define the effective thermal conductivity $\kappa_{\rm eff}$ as

$$\kappa_{\rm eff} = \kappa + \gamma T^3 = \kappa + \frac{16n^2\sigma}{3\beta}T^3. \tag{5}$$

Equation (4) can be reduced to

$$\boldsymbol{J}_{\rm total} = -\kappa_{\rm eff}\nabla T. \tag{6}$$

As suggested by the uniqueness theorem [24], if we can match the boundary conditions between the shell and background artificially, the background temperature profile can be effectively manipulated. To ensure invisibility, we should always keep the background temperature profile (or heat flux) undistorted (see figs. 1(a2) and 1(b2)), so the temperature distribution can be designed as

$$\begin{aligned} (\nabla T)_x &= \nabla T_0, \\ (\nabla T)_y &= 0, \end{aligned} \tag{7}$$

where ∇T_0 is the background thermal gradient, $(\nabla T)_x$ and $(\nabla T)_y$ are the horizontal and vertical thermal gradients in the shell, respectively. We then require to derive the parameters of the shell to satisfy eq. (7). For a cloak, there is an insulated layer outside the object which can block the heat flux. Therefore, according to the heat flux conservation (see fig. 1(a3)), we can achieve

$$\begin{aligned} -\kappa_{{\rm eff1},xx}\left(l_{\rm s}(x) - l_{\rm c}(x)\right)\left|(\nabla T)_x\right| &= -\kappa_{\rm eff,b} l_{\rm s}(x)\left|\nabla T_0\right|, \\ -\kappa_{{\rm eff1},yy} l_{\rm s}(x)\left|(\nabla T)_y\right| &= \delta, \end{aligned} \tag{8}$$

where $\kappa_{\rm eff,b}$ is the effective thermal conductivity of the background, $\kappa_{{\rm eff1},xx}$ (or $\kappa_{{\rm eff1},yy}$) is the horizontal (or vertical) effective thermal conductivity of the shell, and δ has a nonzero value. Since the heat flux requires to bypass the object, the vertical heat flux is nonzero. $l_{\rm s}(x)$ and $l_{\rm c}(x)$ are the exterior and interior widths of the shell at the position x, respectively. We can then derive the effective thermal conductivity of the shell $\kappa_{\rm eff1}$ through eq. (7) and eq. (8) as

$$\kappa_{\rm eff1} = \begin{pmatrix} \dfrac{l_{\rm s}(x)}{l_{\rm s}(x) - l_{\rm c}(x)}\kappa_{\rm eff,b} & 0 \\ 0 & \kappa_{{\rm eff1},yy} \end{pmatrix}, \tag{9}$$

where $\kappa_{{\rm eff1},yy}$ should be ∞ theoretically to ensure that δ is nonzero. With eq. (5), we can rewrite eq. (9) in detail

$$\kappa_{\rm eff1} = \begin{pmatrix} \dfrac{l_{\rm s}(x)}{l_{\rm s}(x) - l_{\rm c}(x)}\left(\kappa_{\rm b} + \dfrac{16n^2\sigma}{3\beta_{\rm b}}T^3\right) & 0 \\ 0 & \kappa_{1,yy} + \dfrac{16n^2\sigma}{3\beta_{1,yy}}T^3 \end{pmatrix}, \tag{10}$$

where $\kappa_{\rm b}$ and $\beta_{\rm b}$ are the thermal conductivity and the Rosseland mean extinction coefficient of the background, respectively. $\kappa_{1,yy}$ and $\beta_{1,yy}$ are, respectively, the vertical thermal conductivity and the Rosseland mean extinction coefficient of the shell, which should be ∞ and 0,

respectively. The shell can then be designed with eq. (10), which does not depend on the shapes of the shell. In other words, the shell can be designed with complex shapes.

We then design an invisible sensor which is slightly different from the invisible cloak. As shown in figs. 1(b1) and (b2), the insulated layer is removed, so heat flux conservation (see fig. 1(b3)) can be expressed as

$$\begin{aligned}&-\kappa_{\mathrm{eff2},xx}\left(l_{\mathrm{s}}\left(x\right)-l_{\mathrm{c}}\left(x\right)\right)\left|\left(\nabla T\right)_x\right|-\kappa_{\mathrm{eff,o}}l_{\mathrm{c}}\left(x\right)\left|\left(\nabla T\right)_x\right|=\\&-\kappa_{\mathrm{eff,b}}l_{\mathrm{s}}\left(x\right)\left|\nabla T_0\right|,\\&-\kappa_{\mathrm{eff2},yy}l_{\mathrm{s}}\left(x\right)\left|\left(\nabla T\right)_y\right|=\delta,\end{aligned}\tag{11}$$

where $\kappa_{\mathrm{eff,o}}$ is the effective thermal conductivity of the sensor. We then use the same method to derive the effective thermal conductivity κ_{eff2} of the shell which satisfies eq. (7),

$$\kappa_{\mathrm{eff2}}=\begin{pmatrix}\dfrac{l_{\mathrm{s}}\left(x\right)\kappa_{\mathrm{eff,b}}-l_{\mathrm{c}}\left(x\right)\kappa_{\mathrm{eff,o}}}{l_{\mathrm{s}}\left(x\right)-l_{\mathrm{c}}\left(x\right)} & 0\\ 0 & \kappa_{\mathrm{eff2},yy}\end{pmatrix},\tag{12}$$

which can be expressed in detail as

$$\kappa_{\mathrm{eff2}}=\begin{pmatrix}\dfrac{l_{\mathrm{s}}\left(x\right)\kappa_{\mathrm{eff,b}}-l_{\mathrm{c}}\left(x\right)\left(\kappa_{\mathrm{o}}+\frac{16n^2\sigma}{3\beta_{\mathrm{o}}}T^3\right)}{l_{\mathrm{s}}\left(x\right)-l_{\mathrm{c}}\left(x\right)} & 0\\ 0 & \kappa_{2,yy}+\dfrac{16n^2\sigma}{3\beta_{2,yy}}T^3\end{pmatrix},\tag{13}$$

where $\kappa_{\mathrm{eff,b}}=\kappa_{\mathrm{b}}+\left(16/3\right)n^2\sigma\beta_{\mathrm{b}}^{-1}T^3$, κ_{o} is the thermal conductivity of the sensor, and β_{o} is the Rosseland mean extinction coefficient of the sensor. $\kappa_{\mathrm{eff2},yy}$ should also be ∞, indicating that $\kappa_{2,yy}$ and $\beta_{2,yy}$ require to be ∞ and 0, respectively. Similarly, eq. (13) does not depend on the shapes of the shell.

Simulations of multithermally invisible cloaks. – We perform finite-element simulations with COMSOL Multiphysics (`http://www.comsol.com/`) to confirm our theory. We set the relative refractive index of all regions as 1 for brevity and set the background size as $8\times8\,\mathrm{cm}^2$ whose thermal conductivity and the Rosseland mean extinction coefficient are $1\,\mathrm{W\ m^{-}1\ K^{-1}}$ and $100\,\mathrm{m}^{-1}$, respectively. These parameters are close to practical materials such as organic glasses, which satisfy the requirements of the Rosseland diffusion approximation.

In the presence of the same temperature field, the radiative flux $\boldsymbol{J}_{\mathrm{rad}}$ is proportional to T^3, but the conductive flux $\boldsymbol{J}_{\mathrm{con}}$ is independent of concrete temperature, as described by eqs. (2) and (3). Therefore, the total heat flux is dominated by radiation at high temperatures. We then apply three temperature intervals to show that the cloak designed with eq. (10) can work under different temperatures. In other words, our scheme can work for both conduction and radiation. The three temperature intervals are: 1) 273–313 K, where conduction is dominant; 2) 273–673 K, where conduction and radiation are roughly equal; 3) 273–2000 K, where radiation is dominant.

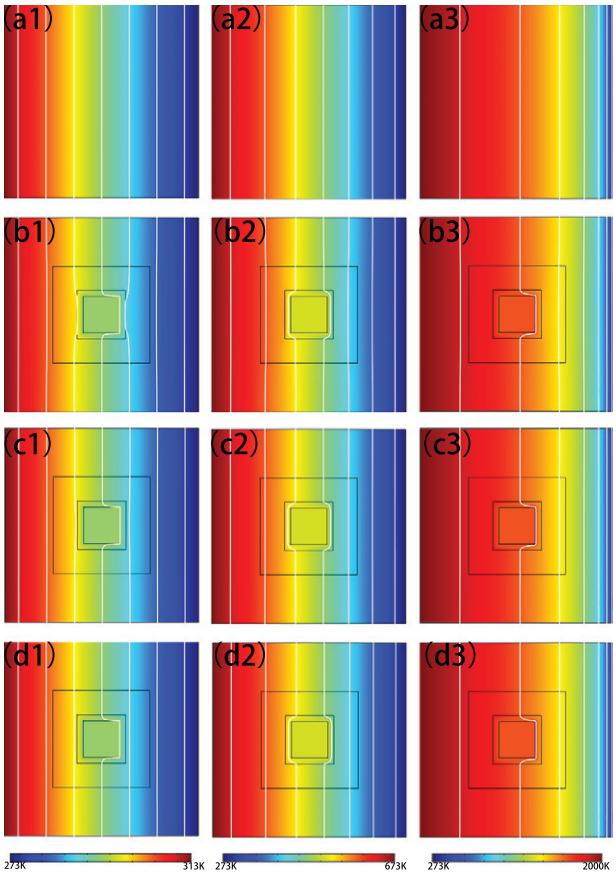

Fig. 2: Simulation results of a square invisible cloak. Color surfaces denote temperature distributions, and white lines represent isotherms. The temperatures of the left boundaries are 313 K, 673 K, and 2000 K, and those of the right boundaries are 273 K. (a1)–(a3) Pure background whose size is $8\times8\,\mathrm{cm}^2$. The thermal conductivity and the Rosseland mean extinction coefficient of background are $1\,\mathrm{W\ m^{-1}\ K^{-1}}$ and $100\,\mathrm{m}^{-1}$, respectively. (b1)–(d3) Object with thermal conductivity $397\,\mathrm{W\ m^{-1}\ K^{-1}}$, the Rosseland mean extinction coefficient $6.5\,\mathrm{m}^{-1}$, and size $1.5\times1.5\,\mathrm{cm}^2$ coated by an insulated layer with thermal conductivity $10^{-5}\,\mathrm{W\ m^{-1}\ K^{-1}}$, the Rosseland mean extinction coefficient $10^5\,\mathrm{m}^{-1}$, and size $2\times2\,\mathrm{cm}^2$. The size of the shell is $4\times4\,\mathrm{cm}^2$. The effective thermal conductivity of the shell is derived from eq. (10). The vertical thermal conductivity $\kappa_{1,yy}$ and the vertical Rosseland mean extinction coefficient $\beta_{1,yy}$ of the shells from the second row to the fourth row are 20, 100, $500\,\mathrm{W\ m^{-1}\ K^{-1}}$ and 5, 1, $0.2\,\mathrm{m}^{-1}$, respectively.

The simulation results are displayed in fig. 2. Figures 2(a1)–(a3) show the homogeneous backgrounds with linear thermal fields under different temperature intervals. We coat the object with an insulated layer, and then add a square shell designed by eq. (10) with

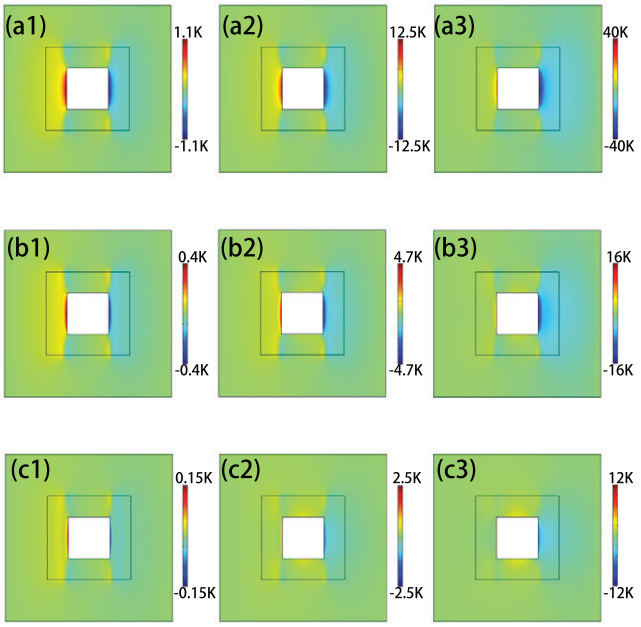

Fig. 3: Temperature differences between figs. 2(b1)–(d3) and the reference group (figs. 2(a1)–(a3)). It is a one-to-one match between figs. 3(a1)–(c3) and figs. 2(b1)–(d3). White regions are occupied by insulated layers which are not of our concern.

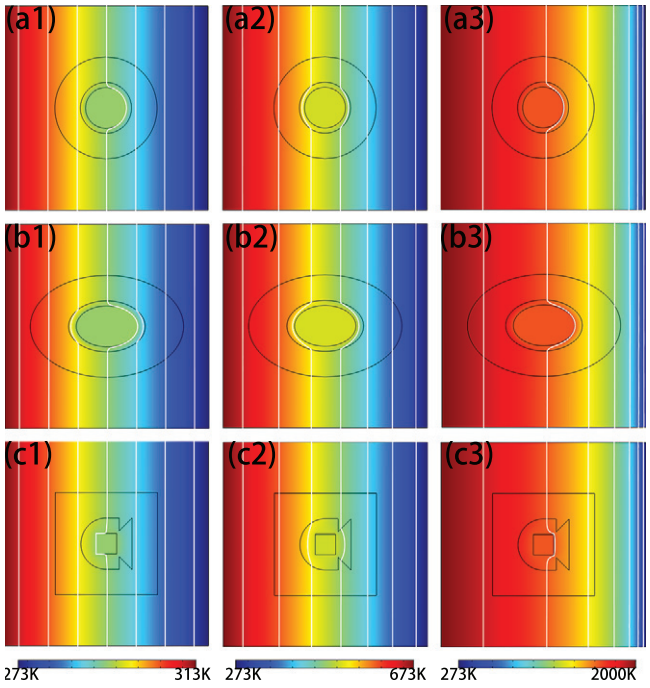

Fig. 4: Simulation results of other shaped cloaks. (a1)–(a3) Circular case. The radii of the shell, insulated layer, and object are 2, 1 and 0.8 cm, respectively. (b1)–(b3) Elliptical case. Semimajor axes of the shell, insulated layer, and object are 3, 1.5 and 1.2 cm, and semiminor axes are 2, 1 and 0.8 cm, respectively. (c1)–(c3) Irregular shape. The shape of the shell is a square while the cavity is fish-like. In all cases, the vertical thermal conductivity of the shells $\kappa_{1,yy}$ is 500 W m^{-1} K^{-1}, and the vertical Rosseland mean extinction coefficient $\beta_{1,yy}$ is 0.2 m^{-1}.

$\kappa_{1,yy} = 20, 100, 500$ W m^{-1} K^{-1} and $\beta_{1,yy} = 5, 1, 0.2$ m^{-1} to remove the temperature distortion. Figures 2(b1)–(d3) exhibit the effects of our device at different temperature intervals, which have almost the same temperature profiles as those in figs. 2(a1)–(a3). Therefore, the object is well hidden, and meanwhile the designed shell is also invisible at different temperature intervals. Moreover, it is clear in fig. 3 that the larger $\kappa_{1,yy}$ and the smaller $\beta_{1,yy}$ yield the better invisibility, which echoes with the prediction of eqs. (9) and (10).

To show the robustness and generality of our theory, we further perform simulations for other shapes. We also coat the object with an insulated layer, and then design the shell with eq. (10). The thermal conductivity of the shell is $\kappa_{1,yy} = 500$ W m^{-1} K^{-1} and the Rosseland mean extinction coefficient is $\beta_{1,yy} = 0.2$ m^{-1}. The desired effects at different temperature intervals are showed in fig. 4, indicating that our theory can be applied to arbitrary shapes.

We then use layered structures composed of two uniform materials to realize the designed invisible cloaks. The effective thermal conductivity (anisotropic) of the shell with layered structure can be written as

$$\kappa_{\rm eff} = \begin{pmatrix} \dfrac{(a+b)\kappa_{\rm a,eff}\kappa_{\rm b,eff}}{a\kappa_{\rm b,eff}+b\kappa_{\rm a,eff}} & 0 \\ 0 & \dfrac{a\kappa_{\rm a,eff}+b\kappa_{\rm b,eff}}{a+b}, \end{pmatrix} \quad (14)$$

where a and b are, respectively, the lengths of the isotropic materials with effective thermal conductivity $\kappa_{\rm a,eff}$ and $\kappa_{\rm b,eff}$. We then choose two materials to fabricate the shell, whose thermal conductivities and the Rosseland mean extinction coefficients are 200 W m^{-1} K^{-1}, 0.5 W m^{-1} K^{-1} and 0.5 m^{-1}, 200 m^{-1}, respectively. In this way, we can specially design the lengths of the two materials according to the theory. The results are shown in fig. 5 with different shapes under different temperature intervals. Clearly, compared to figs. 2 and 4, the layered structures show good effects, indicating that our theory can be applied in experiments.

Simulations of multithermally invisible sensors. – We then show theoretical simulations and experimental suggestions of an invisible sensor. We also set the relative refractive index of all regions as 1 for brevity. The shapes are set to a square and an ellipse. All background parameters are the same as before. A sensor is embedded in the center, whose thermal conductivity and the Rosseland mean extinction coefficient are 0.5 W m^{-1} K^{-1} and 200 m^{-1}, respectively. We also apply

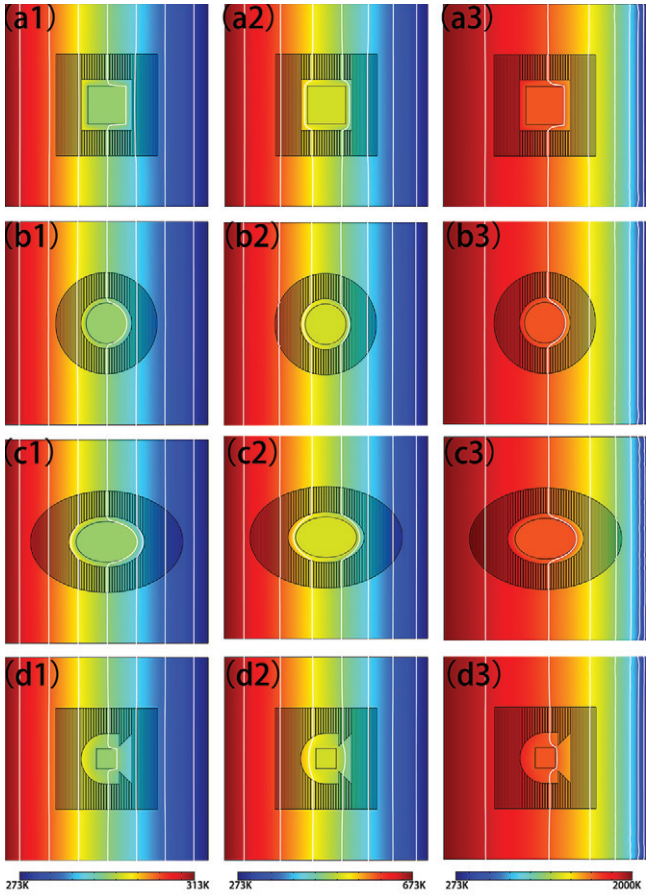

Fig. 5: Experimental suggestions for figs. 2 and 4 with layer structures designed according to eqs. (10) and (14). The parameters are the same as those in figs. 2 and 4. The thermal conductivities and the Rosseland mean extinction coefficients of two materials are $200\,\mathrm{W\ m^{-1}\ K^{-1}}$, $0.5\,\mathrm{W\ m^{-1}\ K^{-1}}$ and $0.5\,\mathrm{m^{-1}}$, $200\,\mathrm{m^{-1}}$, respectively.

three temperature intervals to show that our sensor designed by eq. (13) can work under both high and low temperatures. The thermal conductivity of the shell is $\kappa_{2,yy} = 500\,\mathrm{W\ m^{-1}\ K^{-1}}$ and the Rosseland mean extinction coefficient is $\beta_{2,yy} = 0.2\,\mathrm{m^{-1}}$. The simulation results are displayed in figs. 6(a1)–(a3) and figs. 6(c1)–(c3). As we can observe, our sensors show invisibility in all regions at different temperatures.

Also, we use layered structures composed of two uniform materials to realize our invisible sensors. Thermal conductivities and the Rosseland mean extinction coefficients of the two materials are $100\,\mathrm{W\ m^{-1}\ K^{-1}}$, $0.2\,\mathrm{W\ m^{-1}\ K^{-1}}$ and $1\,\mathrm{m^{-1}}$, $500\,\mathrm{m^{-1}}$, respectively. The lengths of two materials can be specially designed according to eqs. (13) and (14). Figures 6(b1)–(b3) and figs. 6(d1)–(d3) show corresponding simulations with layered structures. These results indicate that our invisible sensors can be fabricated by using two uniform materials, which can be served as experimental suggestions.

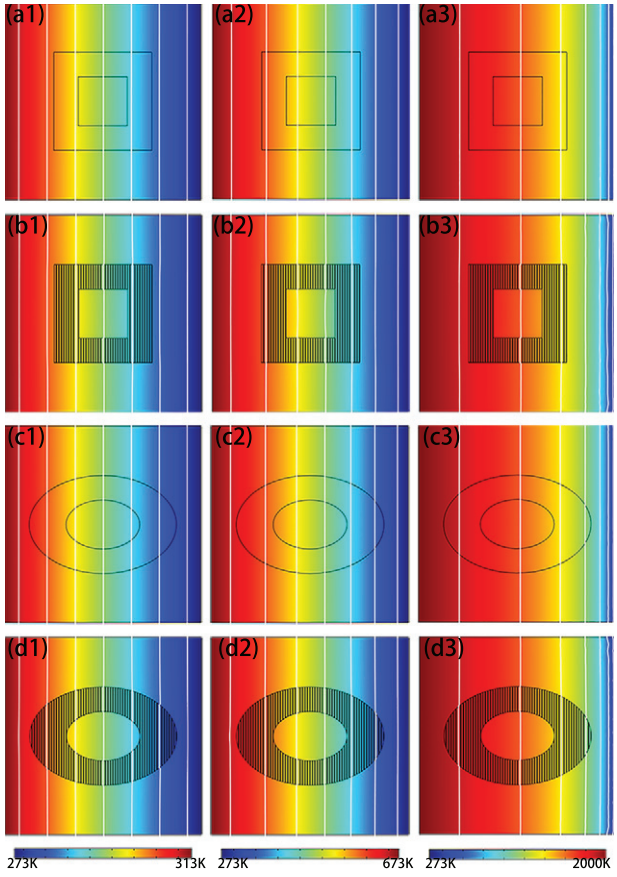

Fig. 6: Simulation results of invisible sensors. (a1)–(a3) Square case. A sensor with thermal conductivity $0.5\,\mathrm{W\ m^{-1}\ K^{-1}}$ and the Rosseland mean extinction coefficient $200\,\mathrm{m^{-1}}$ is directly coated by a square shell with size $4 \times 4\,\mathrm{cm^2}$. The effective thermal conductivity of the shell is derived from eq. (13). (c1)–(c3) Elliptical case. Semimajor axes of the shell and sensor are 3 and 1.5 cm, and semiminor axes are 2 and 1 cm, respectively. The vertical thermal conductivity $\kappa_{2,yy}$ and the vertical Rosseland mean extinction coefficient $\beta_{2,yy}$ of the shells in both cases are $500\,\mathrm{W\ m^{-1}\ K^{-1}}$ and $0.2\,\mathrm{m^{-1}}$. (b1)–(b3) and (d1)–(d3): experimental suggestions for (a1)–(a3) and (c1)–(c3), respectively. Layered structures are designed according to eqs. (13) and (14). Thermal conductivities and the Rosseland mean extinction coefficients of two materials are $100\,\mathrm{W\ m^{-1}\ K^{-1}}$, $0.2\,\mathrm{W\ m^{-1}\ K^{-1}}$ and $1\,\mathrm{m^{-1}}$, $500\,\mathrm{m^{-1}}$.

Discussion and conclusion. – We consider the combination of conduction and radiation in this work. Conduction is handled with the Fourier law which is an appropriate hypothesis at the macroscopic scale. Radiation is dealt with the Rosseland diffusion approximation, indicating that radiative photons travel only a short distance before being absorbed or scattered. With these two assumptions, conduction and radiation can be effectively described by a nonlinear (temperature-dependent) thermal conductivity (eq. (6)), which is convenient for discussion. Certainly, there are many practical materials satisfying these two assumptions like aerogels [41,42].

Furthermore, there are three basic modes of thermal transport in nature, and each way has also different descriptions. Therefore, more extended studies can be expected by considering other mechanisms, such as phononic conduction [43] and near-field radiation [44,45]. Certainly, other methods (which have shown capability in conduction like optimization [46–49]) can also be expected to design multithermal metamaterials. Moreover, the Fourier law (eq. (2)) and the Rosseland diffusion approximation (eq. (3)) are reasonable in steady states, it is also promising to extend these results to transient states by considering mass density and heat capacity [3].

In summary, we have proposed a method based on the thermal uniqueness theorem and the heat flux conservation to design multithermal metamaterials. As practical applications, we have also designed multithermally invisible cloaks and sensors with complex shapes but simple parameters and structures. The feasibility of our scheme is confirmed by finite-element simulations. We also suggest experimental demonstration with layered structures. These results extend the application range of cloaks and sensors, and provide guidance to extend other thermal metamaterials such as concentrators and rotators to multithermotics.

* * *

We acknowledge financial support from the National Natural Science Foundation of China under Grants No. 11725521 and No. 12035004 and from the Science and Technology Commission of Shanghai Municipality under Grant No. 20JC1414700.

REFERENCES

[1] Fan C. Z., Gao Y. and Huang J. P., *Appl. Phys. Lett.*, **92** (2008) 251907.
[2] Chen T. Y., Weng C.-N. and Chen J.-S., *Appl. Phys. Lett.*, **93** (2008) 114103.
[3] Huang J. P., *Theoretical Thermotics: Transformation Thermotics and Extended Theories for Thermal Metamaterials* (Springer) 2020.
[4] Dai G. L., Shang J. and Huang J. P., *Phys. Rev. E*, **97** (2018) 022129.
[5] Li Y., Bai X., Yang T. Z., Luo H. and Qiu C.-W., *Nat. Commun.*, **9** (2018) 273.
[6] Hu R., Huang S. Y., Wang M., Luo X. B., Shiomi J. and Qiu C.-W., *Adv. Mater.*, **31** (2019) 1807849.
[7] Xu L. J., Dai G. L. and Huang J. P., *Phys. Rev. Appl.*, **13** (2020) 024063.
[8] Xu L. J. and Huang J. P., *Int. J. Heat Mass Transf.*, **159** (2020) 120133.
[9] Peng Y.-G., Li Y., Cao P.-C., Zhu X.-F. and Qiu C.-W., *Adv. Funct. Mater.*, **30** (2020) 2002061.
[10] Xu L. J., Yang S., Dai G. L. and Huang J. P., *ES Energy Environ.*, **7** (2020) 65.
[11] Li Y., Zhu K.-J., Peng Y.-G., Li W., Yang T. Z., Xu H. X., Chen H., Zhu X.-F., Fan S. H. and Qiu C.-W., *Nat. Mater.*, **18** (2019) 48.
[12] Xu L. J. and Huang J. P., *Phys. Rev. Appl.*, **12** (2019) 044048.
[13] Yang F. B., Xu L. J. and Huang J. P., *ES Energy Environ.*, **6** (2019) 45.
[14] Yeung W.-S., Mai V.-P. and Yang R.-J., *Phys. Rev. Appl.*, **13** (2020) 064030.
[15] Xu L. J. and Huang J. P., *Sci. China-Phys. Mech. Astron.*, **63** (2020) 228711.
[16] Wang J., Yang F. B., Xu L. J. and Huang J. P., *Phys. Rev. Appl.*, **14** (2020) 014008.
[17] Li Y., Peng Y.-G., Han L., Miri M.-A., Li W., Xiao M., Zhu X.-F., Zhao J. L., Alù A., Fan S. H. and Qiu C.-W., *Science*, **364** (2019) 170.
[18] Cao P. C., Li Y., Peng Y. G., Qiu C. W. and Zhu X. F., *ES Energy Environ.*, **7** (2020) 48.
[19] Xu L. J., Wang J., Dai G. L., Yang S., Yang F. B., Wang G. and Huang J. P., *Int. J. Heat Mass Transf.*, **165** (2021) 120659.
[20] Xu L. J. and Huang J. P., *Appl. Phys. Lett.*, **117** (2020) 011905.
[21] Xu L. J. and Huang J. P., *Chin. Phys. Lett.*, **37** (2020) 080502.
[22] Xu L. J. and Huang J. P., *Chin. Phys. Lett.*, **37** (2020) 120501.
[23] Dede E. M., Yu Z. Q., Schmalenberg P. and Iizuka H., *Appl. Phys. Lett.*, **116** (2020) 191902.
[24] Griffiths D. J., *Introduction to Electrodynamics* (Addison-Wesley) 2007.
[25] Nguyen D. M., Xu H. Y., Zhang Y. M. and Zhang B. L., *Appl. Phys. Lett.*, **107** (2015) 121901.
[26] Lan C. W., Bi K., Gao Z. H., Li B. and Zhou J., *Appl. Phys. Lett.*, **109** (2016) 201903.
[27] Guo J. and Qu Z. G., *Int. J. Heat Mass Transf.*, **127** (2018) 1212.
[28] Xu L. J., Yang S. and Huang J. P., *Phys. Rev. E*, **100** (2019) 062108.
[29] Xu L. J., Yang S. and Huang J. P., *EPL*, **131** (2020) 24002.
[30] Xu L. J., Wang R. Z. and Huang J. P., *J. Appl. Phys.*, **123** (2018) 245111.
[31] Howell J. R., Menguc M. P. and Siegel R., *Thermal Radiation Heat Transfer* (CRC Press) 2010.
[32] Xu H. Y., Shi X. H., Gao F., Sun H. D. and Zhang B. L., *Phys. Rev. Lett.*, **112** (2014) 054301.
[33] Han T. C., Bai X., Gao D. L., Thong J. T. L., Li B. W. and Qiu C.-W., *Phys. Rev. Lett.*, **112** (2014) 054302.
[34] Ma Y. G., Liu Y. C., Raza M., Wang Y. D. and He S. L., *Phys. Rev. Lett.*, **113** (2014) 205501.
[35] Han T. C., Yang P., Li Y., Lei D. Y., Li B. W., Hippalgaonkar K. and Qiu C.-W., *Adv. Mater.*, **30** (2018) 1804019.
[36] He X. and Wu L. Z., *Phys. Rev. E*, **88** (2013) 033201.
[37] Shen X. Y. and Huang J. P., *Int. J. Heat Mass Transf.*, **78** (2014) 1.
[38] Yang T. Z., Bai X., Gao D. L., Wu L. Z., Li B. W., Thong J. T. L. and Qiu C.-W., *Adv. Mater.*, **27** (2015) 7752.
[39] Jin P., Xu L. J., Jiang T., Zhang L. and Huang J. P., *Int. J. Heat Mass Transf.*, **163** (2020) 120437.
[40] Xu L. J., Huang J. P., Jiang T., Zhang L. and Huang J. P., *EPL*, **132** (2020) 14002.

[41] Maleki H., *Chem. Eng. J.*, **300** (2016) 98.
[42] Qu Z. G., Fu Y. D., Liu Y. and Zhou L., *Appl. Therm. Eng.*, **132** (2018) 730.
[43] Bao H., Chen J., Gu X. K. and Cao B. Y., *ES Energy Environ.*, **1** (2018) 16.
[44] Zhang Y., Yi H. L. and Tan H. P., *ACS Photon.*, **5** (2018) 3739.
[45] Zhang Y., Zhou C. L., Qu L. and Yi H. L., *Appl. Phys. Lett.*, **116** (2020) 151101.
[46] Fujii G. and Akimoto Y., *Int. J. Heat Mass Transf.*, **159** (2020) 120082.
[47] Fujii G. and Akimoto Y., *Phys. Rev. X*, **102** (2020) 033308.
[48] Hu R., Iwamoto S., Feng L., Ju S. H., Hu S. Q., Ohnishi M., Nagai N., Hirakawa K. and Shiomi J., *Phys. Rev. X*, **10** (2020) 021050.
[49] Hu R., Song J. L., Liu Y. D., Xi W., Zhao Y. T., Yu X. J., Cheng Q., Tao G. M. and Luo X. B., *Nano Energy*, **72** (2029) 104687.